

See discussions, stats, and author profiles for this publication at: <https://www.researchgate.net/publication/235725923>

Molecular Dynamics Study of Fullerite Cross-Linking under keV C₆₀ and Arn Cluster Bombardment

ARTICLE *in* THE JOURNAL OF PHYSICAL CHEMISTRY C · FEBRUARY 2013

Impact Factor: 4.77 · DOI: 10.1021/jp310635g

CITATIONS

6

READS

45

2 AUTHORS:



Bartłomiej Czerwinski
Luleå University of Technology

28 PUBLICATIONS 562 CITATIONS

[SEE PROFILE](#)



Arnaud Delcorte
Université catholique de Louvain

159 PUBLICATIONS 2,024 CITATIONS

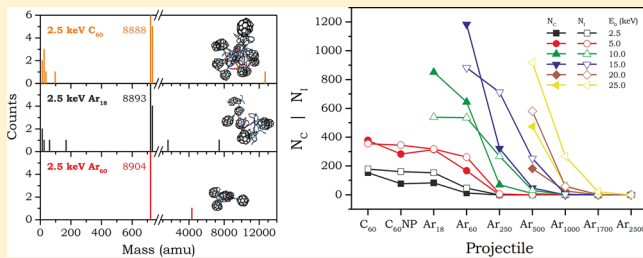
[SEE PROFILE](#)

Molecular Dynamics Study of Fullerite Cross-Linking under keV C_{60} and Ar_n Cluster Bombardment

Bartłomiej Czerwinski* and Arnaud Delcorte

Institute of Condensed Matter and Nanosciences - Bio & Soft Matter (IMCN/BSMA), Université Catholique de Louvain, 1 Croix du Sud, B-1348 Louvain-la-Neuve, Belgium

ABSTRACT: Molecular dynamics computer simulations are used to elucidate the cross-linking processes induced by 0.6–50 keV C_{60} and Ar_n cluster bombardment in a C_{60} fullerite solid sample. The obtained results indicate the presence of a “chemical effect” when C_{60} projectile is used. Namely, the bombarding C_{60} delivers additional, highly reactive, radicals which interact with the atoms of the fullerite sample, increasing the efficiency of the cross-linking process. The omission of those interactions in the analysis makes the C_{60} very similar to the case of the Ar_{18} bombardment. For Ar_n cluster bombardment, the initial energy per atom in the projectile is the parameter which has the predominant influence on the cross-linking process. Furthermore, a relationship between the energy thresholds for fragmentation of the target molecules and cross-linking initiation and the size of the Ar clusters is observed. Both of these thresholds decrease with increasing size of the projectile.



INTRODUCTION

The last few decades of experimental research have brought energetic ion beams to the rank of important processing and characterization tools for a broad segment of the scientific and technological manufacturing sector. Atoms, molecules, and atomic and molecular clusters are nowadays routinely used for surface analysis with the use of techniques like secondary ion mass spectrometry (SIMS),^{1,2} desorption electrospray ionization (DESI) mass spectrometry,^{3–5} or the recently developed desorption ionization by charge exchange (DICE).^{6,7} The main application fields for these techniques are microelectronics, materials science, nanotechnology, and biological research.

A particular acceleration of the development of the SIMS technique occurred along with the introduction of cluster ion guns such as SF_5 , C_{60} , Au_n , Bi_n , and Ar_n . Their implementation allowed to improve the surface characterization of inorganic materials^{8,9} as well as to propose new protocols of analysis for sensitive organic materials and, especially, biological samples.^{1,2} The latest research reveals that ion beams, which utilize large clusters composed of thousands of argon atoms produced by supersonic expansion of high-pressure gas through a nozzle with an energy of a few electronvolts per atom, are able to produce relatively high yields of molecular ions with low (and tunable) fragmentation of the target material.^{10,11} Those ion beams were originally developed for surface smoothing.^{12,13} In addition, unlike SF_5 and C_{60} , the Ar_n clusters are capable of depth profiling most types of organic materials used so far for analysis,² including C_{60} fullerene-based materials,¹⁴ polymers and biological molecules,^{15–17} or multilayered systems.^{18,19} Similarly to their use in the SIMS technique as a tool for analysis of organic surfaces, the fullerene and fullerene-based materials have found their usefulness in the biological and

electronic sciences. For example, functionalized fullerene compounds can be used as mediators in photodynamic killing of cancer cells,²⁰ and their interesting conductivity properties²¹ make them adequate materials for organic electronic and optoelectronic devices²² or new lithium batteries.²³

When an energetic cluster ion interacts with the surface of a carbon-based material, the outcomes are the fragmentation of both projectile and target molecules and the formation of new bonds in the bombarded sample. During the depth-profiling experiments, these processes can be additionally intensified because they are performed in the dynamic SIMS mode. One of the main issues observed during such experiments with, for example, polymers or fullerene-based materials is the fast drop of the characteristic signal of the sample.^{2,14} The observed phenomenon is usually attributed to the formation of cross-links within the bombarded sample and/or the carbonization of its surface.^{2,14,24} In general the cross-linking process is understood as the formation of new bonds between different molecules or polymeric chains, which usually leads to the creation of large chunks of newly bonded material and to the significant reduction of the sputtering efficiency. On the other hand, the term “carbonization” refers to the formation of an amorphous carbon layer in the surface. Carbonization is the end result of extensive dehydrogenation and cross-linking in organic samples. With continuous bombardment, this compact structure can significantly increase its volume and, as a consequence, begin to block the emission of organic material located below. Polystyrene and C_{60} fullerite solid, for example,

Received: October 26, 2012

Revised: January 17, 2013

Published: January 29, 2013

are known as materials readily subject to the polymerization and/or carbonization processes.^{2,24} One recent study confirmed that the depth-profiling analysis of C₆₀ and C₆₀/phthalocyanine layers fails when the C₆₀ ion beam is used for sputtering.¹⁴ Therefore, we chose a C₆₀ fullerite solid as a model sample for the study of cross-linking in this article.

At the beginning of the 1990s, Girifalco analyzed the molecular properties of fullerite by use of molecular dynamics (MD) methods,²⁵ giving some new indications to handle the simulations of fullerite films. His research was, *inter alia*, followed by a study concerning the irradiation of a small C₆₀ sample by keV argon atom bombardment, done by Hobday et al.²⁶ Their work describes one of the first atomistic analyses of Ar atom interactions with a fullerite solid, with the final conclusion that the fullerite solid undergoes polymerization upon irradiation. During the past decade, two studies concerning the interaction of clusters with fullerite samples have been reported by German and Japanese groups.^{27,28} In the first work Anders et al. discuss the fragmentation and ranges of C₆₀ cluster projectiles for different materials, including fcc C₆₀ fullerite, and their dependence on the projectile energy.²⁷ The second study is devoted to the irradiation of carbon-based materials, i.e., fullerite, graphite, and diamond, by (CO₂)_n clusters. The main results of this work are the analysis of the development of the collision cascades in the bombarded materials and the values of sputtering yields as a function of the cluster sizes and initial kinetic energies.²⁸ Recently, Webb et al. reported a similar research for C₆₀ cluster bombardment. Their study focused on the influence of the H:C ratio on the polymerization and cross-linking processes in different organic materials.²⁹ The main conclusion is that the amount of cross-linking induced by C₆₀ increases with decreasing H:C ratio, with the fullerite target being the most cross-linked. To our knowledge, there exists no other theoretical insight into the chemical reaction and cross-linking process which can occur in the fullerene-based materials irradiated by C₆₀ and especially Ar_n cluster projectiles.

In this article, classical MD computer simulations are used as a tool for the investigation of the bond-breaking and the new bond formation processes in a C₆₀ fullerite sample. All the observed phenomena are initiated by the irradiation with C₆₀ and Ar_n ($n = 18, 60, 250, 500, 1000, 1700$, and 2500) clusters with initial kinetic energies in the range of 0.6–50 keV. The total numbers of broken bonds as well as the total numbers of newly created internal and external bonds are analyzed for each bombardment condition. From the theoretical point of view, the formation of new intermolecular bonds at each impact can be regarded as the premise of the cross-linking process which, in the experiments, is observed as the result of continuous ion bombardment of the sample. In this study, we focus on the analysis of a single cluster impact event to compare different cluster projectiles and initial energies and to provide predictions for their use in real world situations.

■ MODEL

This study is conducted using MD computer simulations. The detailed description of the computational procedure can be found elsewhere.³⁰ Briefly, the motion of each particle in the modeled system is determined by integration of Hamilton's equations of motion.³⁰ The forces among the atoms are derived from a blend of pairwise and many-body empirical potentials. The Ar–C interactions are described using the purely repulsive pairwise KrC potential.³¹ To calculate the interactions between

Ar atoms, a Lennard-Jones potential is used.³² It is splined with the KrC potential to properly describe high-energy collisions.³¹ The many-body adaptive intermolecular potential, AIREBO, developed by Stuart and co-workers is used for C–C interactions.³³ This potential is based on the reactive empirical bond order (REBO) potential developed by Brenner et al. for hydrocarbon molecules.³⁴

In addition to its scientific applications and its propensity to cross-link, briefly mentioned in the Introduction, fullerite has been chosen as a model system because of two features, which are important from the technical point of view of this study. Both of them are related to the absence of hydrogen in the system. The first is the significant reduction of the calculation time. For example, the time required to compute 3 ps of 25 keV Ar₅₀₀ bombardment of fullerite sample is almost two times shorter than the time needed to calculate 3 ps of interaction of the same projectile bombarding an amorphous polystyrene sample with 10 times less kinetic energy.³⁵ The second feature concerns the analysis of "chemical reactions" which is much simpler (see below) than in the case of polystyrene because of the absence of hydrogen.³⁵ The basic model approximating the fullerite target contains 1 285 200 carbon atoms, which are arranged in 21 layers of 1020 C₆₀ molecules each (21 420 molecules in total). The size of the sample (303.0 Å × 171.3 Å × 299.6 Å) is chosen to minimize edge effects associated with the dynamical events leading to the ejection of particles. The sample is surrounded by a zone of rigid atoms and a Langevin heat bath region to prevent pressure waves generated by the cluster projectile impact from reflecting off the system boundaries and to keep the sample at the required temperature of 0 K.³⁶ Due to the crystalline structure of the sample, the rigid and stochastic zones have zigzag shape; therefore, their thicknesses can be expressed as (11 ± *r*) and (30 ± *r*) Å, respectively, where the given values correspond to the center of mass of C₆₀ molecules taken into account and *r* is the radius of the single C₆₀. When the larger cluster and/or higher initial energy of the projectile is used for the bombardment, a bigger fullerite model is employed. This second sample contains 2 407 680 carbon atoms arranged in 24 layers of 1672 C₆₀ molecules each (40 128 molecules in total). The sample size is (383.2 Å × 196.1 Å × 386.1 Å), and the rigid and stochastic zones are the same as for the basic model. The surface of both samples is arranged in the fcc{111} configuration. Using information shown in the work of Anders et al.²⁷ and our previous simulations results obtained for a benzene crystal,³⁷ the thickness of the sample was chosen to be almost two times larger than the value of the maximum range of C₆₀ in fullerite. Moreover, the specific shape of both samples (broader than thick) has been chosen in view of the planned simulations with different incidence angles of impinging projectiles. To obtain the proper values of the average lattice constant, measured between the centers of mass of molecules (~14.15 Å)³⁸ and the binding energy of C₆₀ molecules at the equilibrium state of the fullerite solid (~2 eV),^{25,39} small changes in the parameters of the long-range part of the AIREBO potential have been made. The original values of σ and ϵ in the AIREBO's Lennard-Jones potential have been changed from 3.4 Å and 2.844 meV to 3.965 Å and 1.982 meV, respectively. Additionally, the maximum range of the C–C interactions was reduced from 8.9 to 8.1 Å.³³ The density of the sample is ~1.65 g/cm³, which is in good agreement with the experimental value of 1.67 ± 0.02 g/cm³.⁴⁰

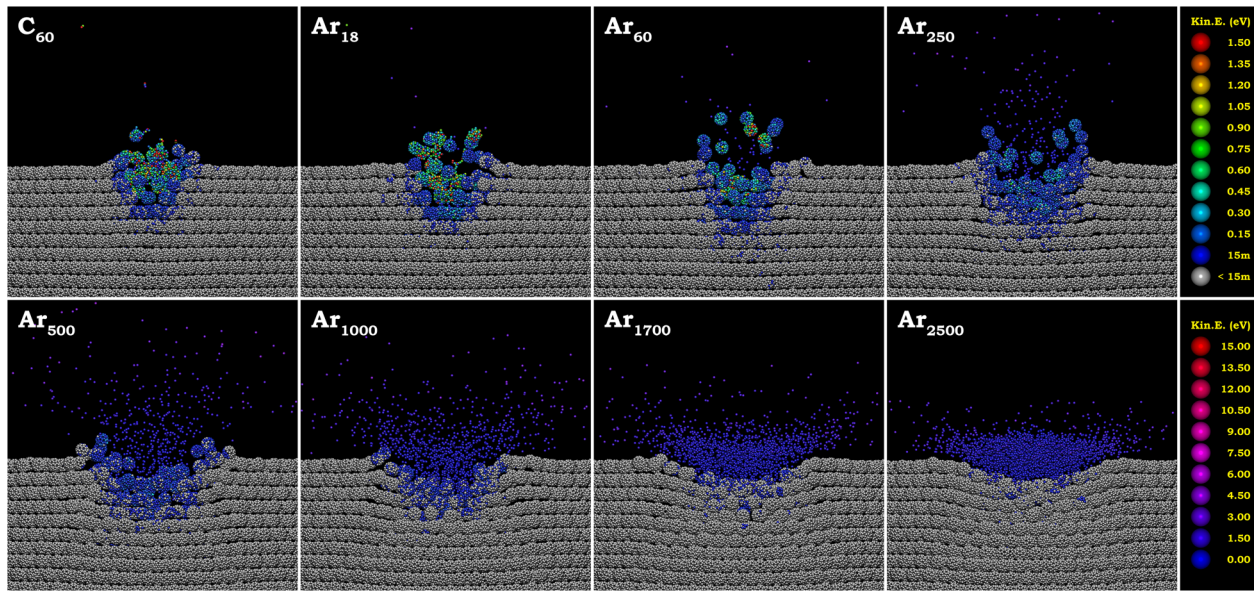


Figure 1. Cross-sectional and zoomed side view of the time evolution snapshots at 3 ps after bombardment with 2.5 keV C_{60} and Ar_n ($n = 18, 60, 250, 500, 1000, 1700$, and 2500) cluster projectiles. The color scales represent the kinetic energy of single substrate (top) or projectile (bottom) atoms.

The fullerite substrate was bombarded by C_{60} and Ar_n ($n = 18, 60, 250, 500, 1000, 1700$, and 2500) cluster projectiles which were directed normal to the surface. To calculate the number of broken bonds and newly created internal and external bonds at each chosen time step ($\Delta t = 100$ fs) of analysis, the list of atoms bonded to each atom in the system was checked and compared to the list of atoms bonded to the same atom in its initial state ($t = 0$ fs). Since the analysis was based on the “snapshots” of the entire system taken from the MD simulations at the predefined time steps, the atoms bonded to each individual atom within the bombarded system were searched based on relative distance between atoms. The threshold value for this distance (maximum search radius) was taken at the half of maximum interaction energy of two carbon atoms in the equilibrium state, as defined by the attractive part of the AIREBO potential.³³ This gave a value of 1.79 Å for C–C interactions. When the list of atoms bonded to each individual atom changed, it was classified as (1) creating a new external bond, if it had a new bonded atom initially originating from the different molecule, as (2) creating a new internal bond, if it had a new bonded atom initially originating from the same molecule, or (3) broken, if the number of bonded atoms was reduced but it did not create any new external or internal bonds. The atom was classified as (4) intact, if its bonded atom list did not change. Additionally, molecules containing different types of atoms were marked according to the same rules, as containing new external bonds, containing new internal bonds, broken, or intact. To speed up the calculations of number of broken and new bonds, the atoms belonging to the rigid and stochastic zones of both samples were not taken into account. Hence, the total number of analyzed atoms was reduced to 534 600 and 1 207 800 for the small and the large sample, respectively. All the analyses shown in this paper were conducted at 3 ps after impact of the projectile. However, some longer time simulations were performed for a few “high energy per atom” cases. The results from those calculations indicate that when a projectile with high energy per atom is used, as for example 25 keV Ar_{500} , a slow but

continued increase of the total number of broken bonds, newly created internal bonds, and cross-links occurs. Nevertheless, we carefully checked that the observed increase has no influence on the final conclusions of this research. For this reason, the time of 3 ps has been chosen for analysis for all the bombardment conditions.

RESULTS AND DISCUSSION

The final result of the interaction of an energetic cluster projectile with a material is the emission of particles from the substrate, which is essentially outside of the time frame of our simulations. In the first few picoseconds of this process the impinging projectile breaks apart, which may lead to the bond breaking in the substrate and eventually to the formation of new bonds. The analysis of bond scissions and new bond creations constitutes the focus of this article. We first provide an overview of the chemistry induced in the solid by the different clusters and, then, investigate the parameters of interest to explain the observed trends.

Structural Modification of the Fullerite Solid. The zoomed cross-sectional view of the fullerite crystal at 3 ps after bombardment by 2.5 keV C_{60} and Ar_n clusters is shown in Figure 1. The observed damage of the sample induced by the Ar_{18} projectile as well as the spatial kinetic energy distribution of substrate atoms is similar to the case of C_{60} cluster bombardment. Even though the crater formation is still ongoing, the observed features are in good agreement with the results obtained for solid benzene.⁴¹ This indicates that the sputtering processes initiated by the C_{60} and small argon clusters, as well as the final shape and volume of the damaged area, should be similar. For C_{60} and small Ar clusters, the sputtering proceeds in a manner known for small cluster projectiles.^{42,43} Briefly, the energy carried by such projectiles is deposited close to the surface of the fullerite solid, initiating collective motion of atoms, which finally leads to the formation of a characteristic, almost hemispherical, crater.⁴³ When larger clusters are used, the lateral size of the damaged region increases while its depth decreases. This is the effect of a

significant change in the manner the projectile interacts with the bombarded sample. Similarly to the case of solid benzene,³⁷ large argon clusters generate pressure waves in the substrate and push molecules down toward the bulk of the sample. However, due to the much higher binding energy of C_{60} molecules in the fullerite solid (~ 2 eV vs ~ 0.5 eV for benzene), the impinging projectile does not have enough energy per atom to break bonds in C_{60} molecules, only leading to the creation of internal excitation. Therefore, we can speculate that, in the later stage of the sputtering process, the behavior of the fullerite sample may be similar to the case of the sec-butyl-terminated polystyrene (PS4) overlayer on silver, where the PS4 molecules (having similar surface binding energy) are ejected due to the collective interaction with atoms of the recovering substrate, which acts as a trampoline.⁴⁴

The differences observed in the initial phase of the bombardment find their confirmation in the mass spectral comparison shown in Figure 2. The presented spectra are

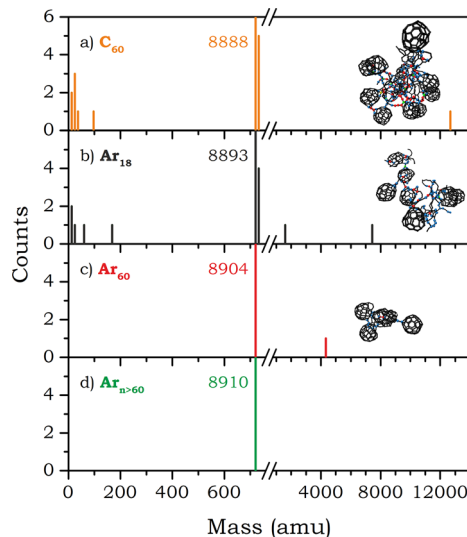


Figure 2. Comparison of mass spectra calculated at 3 ps after bombardment with 2.5 keV C_{60} and Ar_n ($n = 18, 60, 250, 500, 1000, 1700$, and 2500) cluster projectiles. The highlighted values represent the total number of intact C_{60} molecules in the whole analyzed part of the sample, and the inset pictures are the graphic representations of the largest molecules in the spectra.

calculated for the part of the sample considered for the analysis of chemical reactions in the solid (see Model section). The highlighted values represent the number of intact C_{60} molecules in that volume. The mass spectrum obtained for the Ar_{18} bombardment (Figure 2b) exhibits the presence of both fragmented and linked fullerite molecules and is well comparable with the C_{60} case (Figure 2a). For Ar_{60} , the target fragments disappear from the spectrum (Figure 2c) and the molecular cross-linking vanishes for clusters larger than Ar_{60} (Figure 2d). The absence of fragmentation and cross-linking of fullerite molecules observed for large argon clusters confirms that these clusters are not able to overcome the covalent interactions in the fullerite solid with a kinetic energy of 2.5 keV. These results follow the trends observed for the bombardment of the coarse-grained amorphous polyethylene⁴⁵ and solid benzene crystal.⁴⁶ According to these studies the ejection of target fragments is visible only if the energy/nucleon in the projectile is higher than a threshold value, which was

estimated to be ~ 1 eV in the case of coarse-grained polyethylene.⁴⁵ The threshold value in our case seems to be similar, since the energy/nucleon calculated for 2.5 keV Ar_{60} projectile is ~ 1.04 eV and this projectile does not induce any fragmentation of molecules in the fullerite sample. However, the more detailed analysis of the mass spectra, obtained for the other projectiles and initial kinetic energies (not shown), reveals that the threshold value of energy at which fragmentation of target molecules starts decreases with increasing size of the projectile from ~ 1.67 eV/nucleon for Ar_{18} to ~ 0.75 eV/nucleon in the case of Ar_{500} .

The time evolution of the number of bonds broken (N_{BB}) during the first 3 ps of the bombardment of C_{60} fullerite by 2.5 keV C_{60} and Ar_n clusters is shown in Figure 3a. In the case of

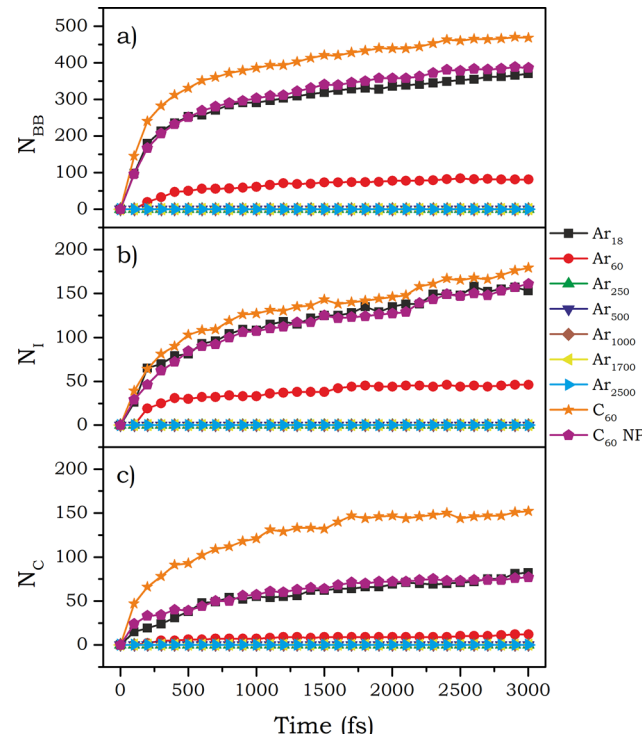


Figure 3. Time evolution of number of bonds broken (a) and created as new internal bonds (b) or cross-links (c) during 2.5 keV C_{60} and Ar_n cluster bombardment of fullerite crystal. The plot tagged as C_{60} NP represents the time evolution in which atoms of the projectile are not taken into account for analysis.

Ar_{60} , most of those bonds are broken during the first 500 fs, and then their number slowly increases to be fully saturated at 3 ps after the impact. For C_{60} and Ar_{18} bombardment, the increase rate of bond breaking is reduced after 500 fs. However, it is not fully saturated before the end of the simulations. At the end of the simulation time, the total number of broken bonds is the highest for C_{60} . Nevertheless, it should be noted that the C_{60} projectile contains 90 C–C bonds which break during the interaction with the surface, and they are included in the calculated values. When the number of bonds broken in the projectile itself is subtracted (the plot line tagged as C_{60} NP), the time evolution curve and the final number of broken bonds become very similar to the case of Ar_{18} cluster bombardment. Similar trends are predicted for the time evolution of new internal bonds (N_I) and cross-links (N_C) created in the system, as shown in Figure 3b and c, respectively. When the final total

numbers of internal bonds and cross-links are compared, it is clear that the ratio of cross-links/internal bonds is much higher in the case of the C_{60} projectile bombardment as compared to Ar_{18} . This is due to the fact that the broken C_{60} projectile provides highly reactive carbon radicals which interact with particles of the fullerite surface, leading to the creation of additional cross-links. When these additional bonds are not taken into account, the total number of broken bonds, new internal bonds, and cross-links created by C_{60} and Ar_{18} projectile can be treated as equal within the limits of the statistical error. These first data obtained for 2.5 keV bombardment of the fullerite crystal already show that the significant increase in the efficiency of the cross-linking process in the case of C_{60} bombardment is due to the presence of highly reactive radicals originating from the decay of the projectile. These results also indicate that the total mass of the projectile seems to be the key parameter explaining the similarity in the cross-link efficiency obtained for C_{60} and Ar_{18} projectiles. If the number of atoms in the Ar_n cluster is increased to values typically used with Ar cluster ion guns (500–5000), the cross-linking of molecules completely disappears. However, it must be noted that 2.5 keV is in the lower energy range of typical SIMS experiments. Therefore, further analysis for higher energy impacts is performed hereafter.

Figure 4a shows the projectile dependent distributions of number of broken bonds obtained for the different initial kinetic energies of the used projectiles. There are two visible trends. First, when the number of atoms (hence the size and the mass) in the Ar cluster increases, the number of broken

bonds decreases, reaching a value close or equal to zero for the large clusters. The second trend is the increase of the number of broken bonds with the increase of the initial kinetic energy of the projectile. This trend is visible for all the used projectiles. However, the initial threshold value of energy for which the bond-breaking process is initiated is different for each projectile. It increases with the projectile nuclearity. The projectile dependent distributions of total numbers of newly created internal bonds and cross-links follow the same general trends (Figure 4b). There are some interesting features, which can be observed when comparing the N_C and N_I distributions. When a constant initial energy is considered, a crossing of the N_C and N_I curves can be observed. For example, for small Ar clusters at 10–15 keV, the number of cross-links created during bombardment is higher than the number of internal bonds. After passing a critical size of the projectile, the number of cross-links becomes lower than the number of internal bonds. The critical size of the projectile can be estimated as 100 and 115 atoms for 10 and 15 keV, respectively. A crossing of the N_C and N_I plots is also observed in the case of 5 keV C_{60} bombardment. In this case, the total number of cross-links created in the fullerite solid is higher than the total number of internal bonds. However, when the bonds created by the projectile are not taken into account in the analysis (points on the right side of the plots tagged with C_{60} NP), the situation becomes opposite. This not only confirms the “chemical effect” of the C_{60} cluster but also shows that for higher initial kinetic energies the impinging C_{60} projectile participates preferentially in the creation of intermolecular bonds between molecules of the fullerite solid (polymerization).

Effect of the Projectile Parameters on the Cross-Linking Process.

To obtain a more detailed insight into the events occurring during the bombardment by Ar clusters of different sizes and constant initial kinetic energy (for example, 10 keV), the initial positions of atoms which create cross-links and new internal bonds have been studied. As shown in Figure 5, the depth and the measured surface area of molecules taking part in the cross-linking (columns 1 and 2), as well as creating new internal bonds (columns 3 and 4), decrease with increasing size of the projectile. This decrease is followed by the change of the initial positions of atoms having one or more cross-links or newly created internal bonds. Starting from the smallest projectile, the initial positions of cross-linking atoms are mainly located along the track of the impacting projectile and in a small rim surrounding this track. When the number of atoms in the projectile increases, the initial positions of cross-linking atoms approach the impact point and become located straight under the projectile. The evolution is similar for new internal bonds. For Ar_{18} , the initial positions of internally bonding atoms are located in the $\sim 15 \text{ \AA}$ wide rim surrounding the track of the impacting projectile. Increasing the size of the projectile leads to the decrease of the internal radius and the width of the rim. Ultimately, this area is located straight under the projectile as it was in the case of the cross-linking atoms. The changes of initial positions of chemically reactive atoms, when the A_{60} projectile is replaced by the larger Ar_{250} , are connected with the crossing of the N_C and N_I plots (Figure 4b). However, it still not clear which parameter of the projectile has the highest impact on the observed phenomena. In order to clarify this issue, an additional analysis for the constant size (mass) of the projectile and constant initial kinetic energy per atom in the cluster has been performed.

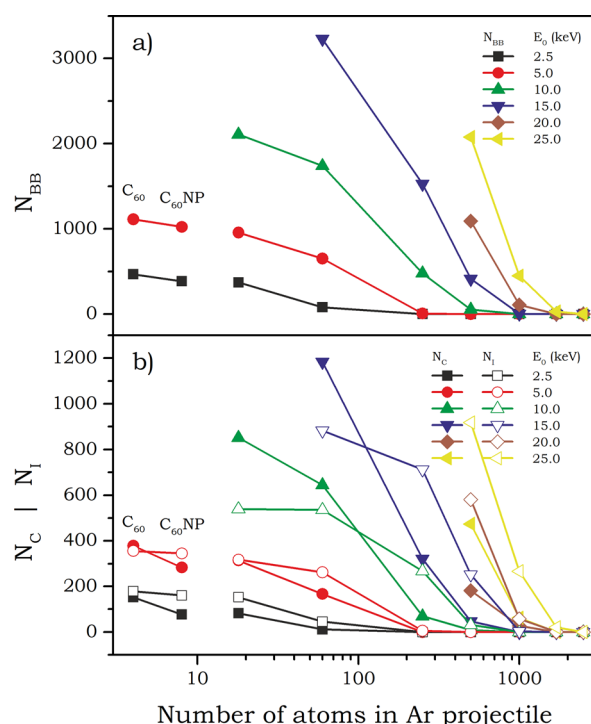


Figure 4. Projectile dependent distributions of (a) the total number of broken bonds (N_{BB}) and (b) the total number cross-links (N_C) and newly created internal bonds (N_I) obtained for different initial kinetic energies. The plots for C_{60} cluster bombardment are shown for comparison, and they are not in proper scale with the horizontal axis. The points tagged as $C_{60}NP$ represent the situation in which atoms of the projectile are not taken into account in calculation of N_{BB} , N_C , and N_I .

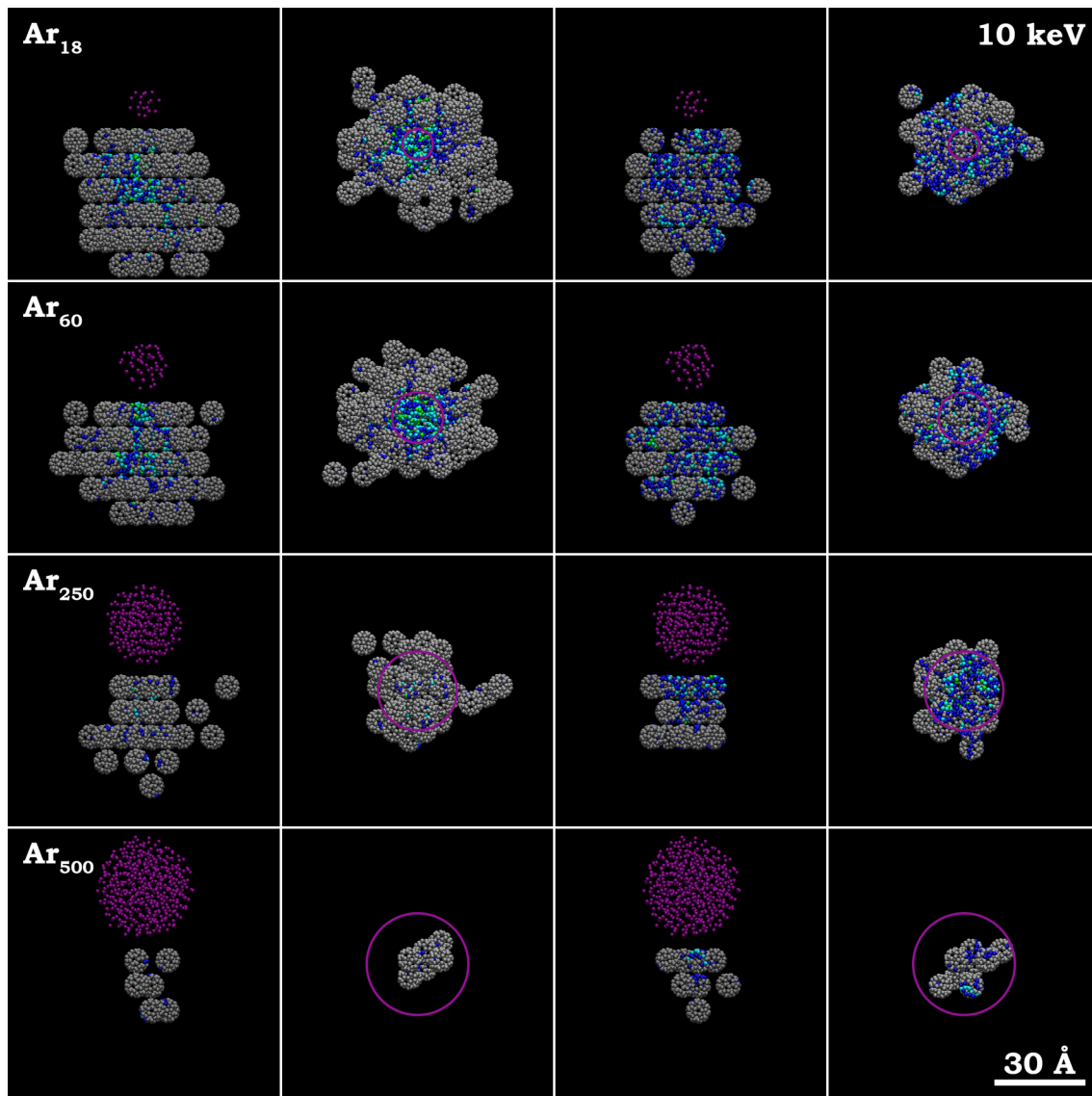


Figure 5. Side (column 1 and 3) and top view (column 2 and 4) of the initial positions of cross-linking (column 1 and 2) and newly internal bonded (column 3 and 4) atoms in fullerite sample bombarded by different argon clusters with initial energy of 10 keV. Only molecules involved in chemical reactions are shown. Colors represent the number of newly created cross-links or internal bonds: gray, 0; blue, 1; cyan, 2; green, 3; yellow, 4. The circle represents the maximum radius of the projectile.

As shown in Figure 4 the intersection of N_C and N_I plots is observed also for a constant number of atoms in the projectile. For example, in the case of Ar_{60} , the threshold value of energy at which the curve crossing occurs is located between 5 and 10 keV. As was the case at constant initial kinetic energy, the intersection of the total number of cross-links and newly created internal bonds is followed by the different evolution of the shape of the regions where the highest intensity of cross-linking and/or new internal bonding occurs (Figure 6). For the initial kinetic energy 5 keV or lower, both of these regions have an elongated shape and are located along the track of the projectile. When the energy is increased to 10 keV or more, the lateral radius of these regions increases. However, in the case of cross-linking molecules the highest intensity of atoms having larger number of cross-links is still located mainly along the track of the projectile with a few atoms located randomly in the outer rim of this region, while for the case of internal bonding the horizontal cross section of the high-intensity region becomes more annular with the inner boundary radius close

to the radius of the projectile. The total number of atoms creating new internal bonds which are located along its track is highly reduced. The threshold value of energy per atom at which the change of shape of the region containing new internal bonds occurs is between 83.3 and 166.7 eV/atom which corresponds to the energy of 2.08 and 4.17 eV/nucleon, respectively.

The final point of our analysis concerns the dependence of the chemical processes occurring in the fullerite sample on the change of the size and the total initial energy of the impinging cluster when the initial energy per atom/nucleon is kept constant. The projectile dependent distributions of total numbers of broken bonds, newly created internal bonds, and cross-links calculated for the energy of 20 eV/atom (0.5 eV/nucleon) are shown in Figure 7. There are two main features visible in the picture. First, the total numbers of broken bonds, cross-links, and newly created internal bonds increase with the number of atoms in the projectile. Second, the number of newly created internal bonds has a higher value than the

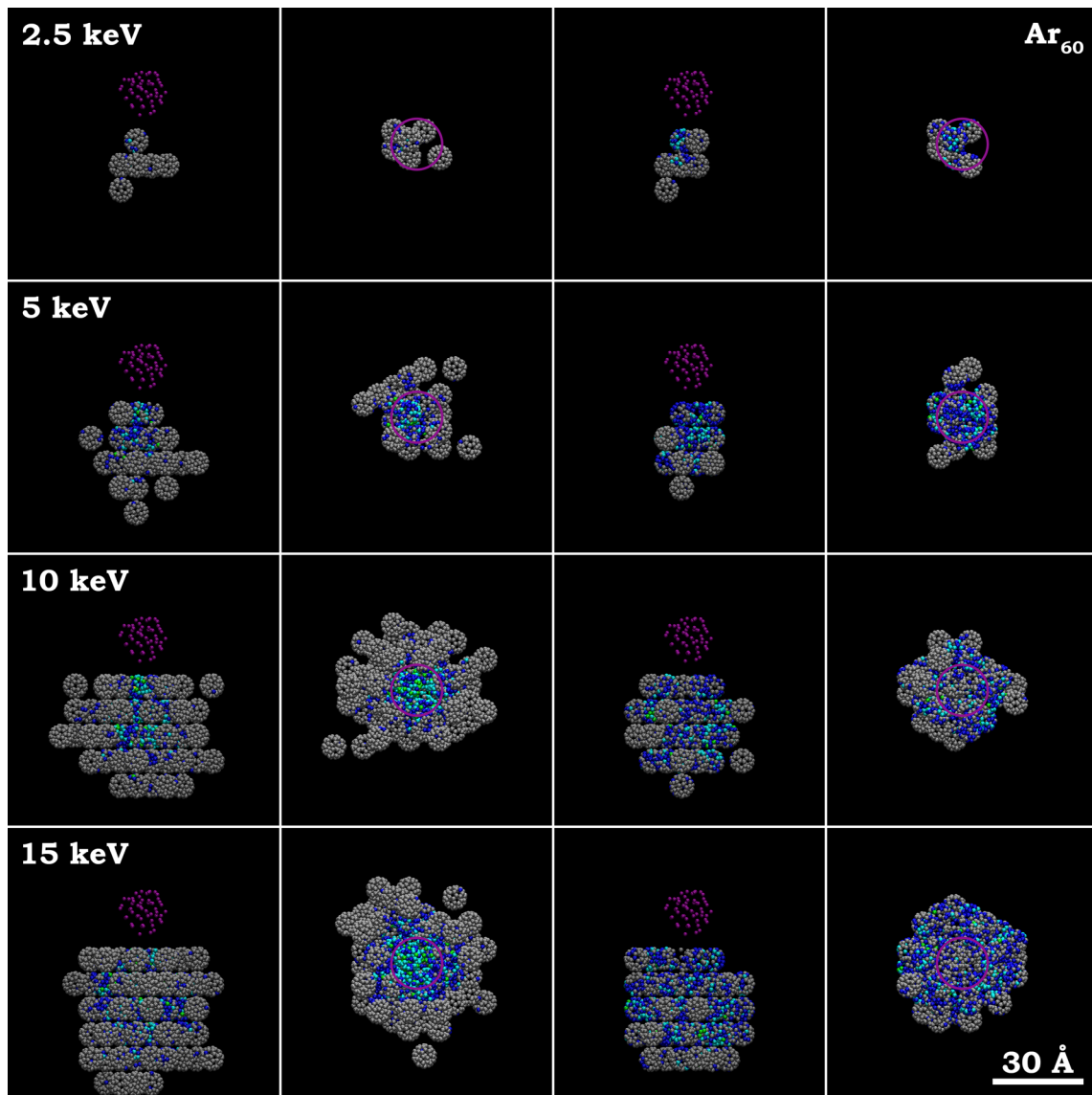


Figure 6. Side (column 1 and 3) and top view (column 2 and 4) of the initial positions of cross-linking (column 1 and 2) and newly internal bonded (column 3 and 4) atoms in fullerite sample bombarded by Ar_{60} cluster with different initial energies. Only molecules involved in chemical reactions are shown. Colors represent the number of newly created cross-links or internal bonds: gray, 0; blue, 1; cyan, 2; green, 3; yellow, 4. The circle represents the maximum radius of the projectile.

number of new cross-links, and the N_C and N_I plots do not cross, unlike what was seen for the case of constant size of the cluster or constant total initial energy (as shown in Figure 4). The first trend can be attributed to the increased area where the chemical reactions can occur, proportional to the projectile size. The second feature can be easily attributed to the value of energy per atom chosen for this analysis, which is in the domain where $N_I > N_C$.

The step by step analysis leads us to the conclusion that all the parameters of the projectile have an influence on the chemical reactions occurring in the bombarded fullerite solid. However, in terms of cross-linking process, defined as the creation of bonds between atoms belonging to different molecules (large clusters visible in the mass spectra), the most influential parameter is the initial energy per atom (or energy per nucleon) in the projectile, which is followed by the size of the cluster. The energy per nucleon dependent distributions of the $N_{BB}/\text{nucleon}$, $N_I/\text{nucleon}$, and $N_C/\text{nucleon}$

are presented in Figure 8. All the argon clusters exhibit a similar increase of these parameters with increasing energy per nucleon. A one order of magnitude energy change leads to almost 5 orders of magnitude enhancement of the total number of broken bonds and newly created internal bonds, as well as almost 4 orders of magnitude enhancement of cross-link creation. The obtained results also indicate that, in the case of Ar_{500} and larger clusters, the minimal energy of ~ 0.5 eV/nucleon needed to initiate the cross-linking process is lower than the threshold energy (~ 0.75 eV/nucleon) of fragmentation of fullerite molecules. Both of these threshold energy values increase with the decrease of size of the impinging projectile, reaching similar values of ~ 1.67 eV/nucleon for the Ar_{18} case. This proves that the cross-linking process is also influenced by the size of the cluster used for bombardment.

Comparison with an Hydrocarbon Target. There are several similarities and differences between the 2.5 keV C_{60} and Ar_n cluster bombardment of fullerite and that of an amorphous

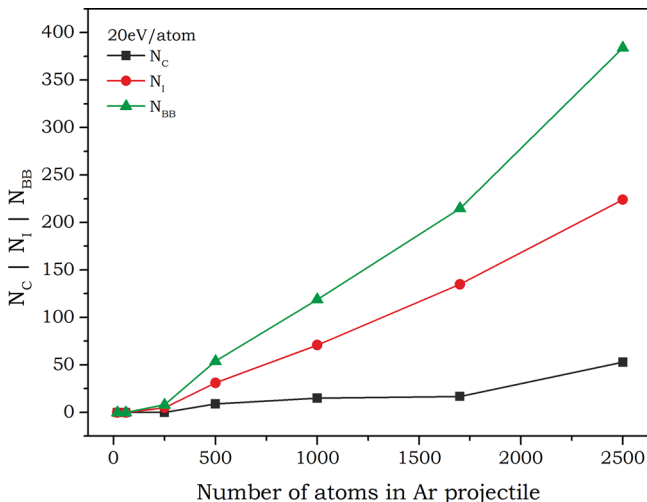


Figure 7. Projectile dependent distributions of the total number of broken bonds (green), the total number of cross-links (black), and newly created internal bonds (red) obtained for the constant energy per atom (20 eV/atom).

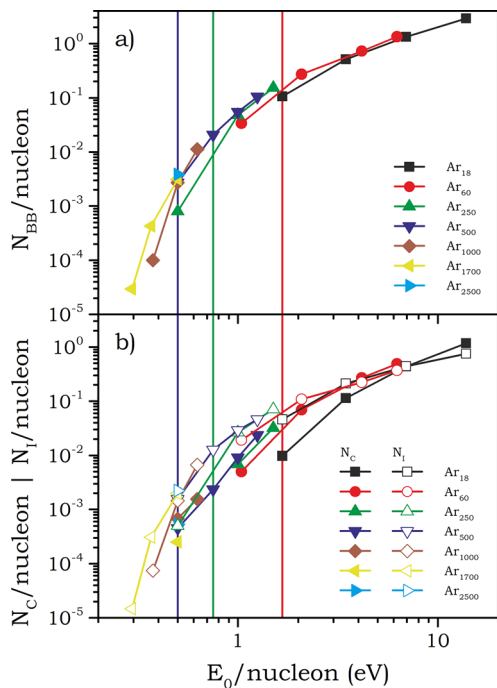


Figure 8. Dependence of the total number of (a) broken bonds and (b) cross-links and new internal bonds per nucleon on the initial energy per nucleon. The colored lines represent the threshold values of energy/nucleon when fragmentation of target molecules and cross-linking for Ar_{18} projectile (red), fragmentation of target molecules (green), and cross-linking (blue) for Ar_{500} and larger clusters are initialized in the bombarded fullerite solid.

sec-butyl-terminated polystyrene (aPS4) sample.³⁵ First, the craters formed in the aPS4 surface, at 3 ps after bombardment, have similar diameters, but their depths are ~2 times larger as compared to the craters formed in the fullerite solid. This is essentially due to the different density of the materials, which are ~1.65 and ~1.04 kg/dm³ for fullerite and aPS4, respectively. Second, the time evolution of the bond-breaking and new bond formation processes look similar even though the increase of the number of chemical reactions in the initial

phase (first 500 fs) of the sputtering process is more intense in the case of the fullerite solid. Third, the final number of cross-links created in the fullerite is up to 7.5 times larger than in the case of the aPS4 sample. This is in good agreement with the research performed by Webb et al.²⁹ concerning C_{60} impacts on carbon-based materials, confirming that the presence of hydrogen in the sample reduces the number of induced cross-links. Finally, the volumes of molecules taking part in chemical reactions are similar for both samples (when there is new bond formation). This is the consequence of the similar energy transfer rates between projectile and surface atoms.

CONCLUSION

Our results indicate that the main effect differentiating C_{60} from Ar_n cluster irradiation is the “chemical effect” of the projectile. The C_{60} molecule breaks up into a maximum of 60 highly reactive carbon radicals upon impact. Each of these radicals can react with a maximum of four elements from its closest neighborhood, which could induce a maximum of 240 new bonds, in the most extreme case. Our results show that the numbers of newly created external bonds originating from this chemical effect are 75 and 95 for the energies of 2.5 and 5 keV, respectively. This constitutes ~49% and ~25% of the total number of created cross-links. The observed effect affects mainly the intermolecular bonding process. When this chemical effect is excluded from analysis, the values of all the calculated quantities become comparable with those obtained for the Ar_{18} cluster bombardment, which has a similar total mass and volume. This implies a similar efficiency of the Ar_{18} projectile in terms of chemical reactions as the C_{60} cluster devoid of its chemical reactivity.

The analysis of the Ar cluster impacts, with different sizes and initial total kinetic energies, reveals that the parameter which has the prevalent impact on the chemical reactions occurring in the bombarded fullerite sample is the initial energy per atom of the projectile. Increasing the energy per atom by just 1 order of magnitude leads to almost 5 orders of magnitude enhancement of the bond-breaking process and, as a consequence, to almost 4 orders of magnitude increase of the total number of created cross-links. A relationship between the energy per nucleon thresholds for fragmentation of target molecules and cross-linking and the size of the projectile is also found. Namely, both energy thresholds decrease with increasing size of the projectile. The thresholds of these two processes are similar in the case of small argon clusters, ~1.67 eV/nucleon. When the size of the projectile increases, the thresholds separate and their values are reduced to ~0.75 and ~0.5 eV/nucleon for fragmentation of fullerite molecules and cross-linking, respectively. This means that the cross-linking can occur without visible fragmentation of target molecules in the mass spectrum. Additionally, we find that the bond breaking and creation of new internal bonds can occur even below the cross-linking threshold, meaning that in some cases the intramolecular reorganization of bonds will not be seen in the experimental mass spectrum at all. The comparison with a polystyrene sample reveals that the structural properties of the two materials are responsible for the differences observed in terms of chemical reactions and cross-linking efficiency.

AUTHOR INFORMATION

Corresponding Author

*Phone: +3210478460. Fax: +3210473452. E-mail: bartlomiej.czerwinski@uclouvain.be

Notes

The authors declare no competing financial interest.

ACKNOWLEDGMENTS

The authors thank B. J. Garrison (Penn State University, PA), R. P. Webb (University of Surrey, U.K.), and Z. Postawa (Jagiellonian University, Poland) for the inspiring and productive scientific discussions during the realization of this project. The Belgian Fonds National pour la Recherche Scientifique (FNRS) and the European Union, through the 3D nanochemiscope convention, are acknowledged for financial support. Computational resources have been provided by the supercomputing facilities of the Université Catholique de Louvain (CISM/UCL) and the Consortium des Equipements de Calcul Intensif en Fédération Wallonie Bruxelles (CECI) funded by the Fond de la Recherche Scientifique de Belgique (FRS-FNRS). A.D. is a Senior Research Associate of the FNRS.

REFERENCES

- (1) Winograd, N. The Magic of Cluster SIMS. *Anal. Chem.* **2005**, *77*, 142A–149A.
- (2) Mahoney, C. M. Cluster Secondary Ion Mass Spectrometry of Polymers and Related Materials. *Mass Spectrom. Rev.* **2010**, *29*, 247–293.
- (3) Takats, Z.; Wiseman, J. M.; Gologan, B.; Cooks, R. G. Mass Spectrometry Sampling Under Ambient Conditions with Desorption Electrospray Ionization. *Science* **2004**, *306*, 471–473.
- (4) Meetani, M. A.; Shin, Y. S.; Zhang, S.; Mayer, R.; Basile, F. J. Desorption Electrospray Ionization Mass Spectrometry of Intact Bacteria. *Mass Spectrom.* **2007**, *42*, 1186–1193.
- (5) Laskin, J.; Heath, B. S.; Roach, P. J.; Cazares, L.; Semmes, O. J. Tissue Imaging Using Nanospray Desorption Electrospray Ionization Mass Spectrometry. *Anal. Chem.* **2012**, *84*, 141–148.
- (6) Chan, C. C.; Bolgar, M. S.; Miller, S. A.; Attygalle, A. B. Desorption Ionization by Charge Exchange (DICE) for Sample Analysis Under Ambient Conditions by Mass Spectrometry. *J. Am. Soc. Mass Spectrom.* **2010**, *21*, 1554–1560.
- (7) Chan, C. C.; Bolgar, M. S.; Miller, S. A.; Attygalle, A. B. A Combined Desorption Ionization by Charge Exchange (DICE) and Desorption Electrospray Ionization (DESI) Source for Mass Spectrometry. *J. Am. Soc. Mass Spectrom.* **2011**, *22*, 173–178.
- (8) Sun, S.; Szakal, C.; Smiley, E. J.; Postawa, Z.; Wucher, A.; Garrison, B. J.; Winograd, N. Sputtering of Ag under C_{60}^+ and Ga^+ Projectile Bombardment. *Appl. Surf. Sci.* **2004**, *231*–232, 64–67.
- (9) Sostarecz, A. G.; Sun, S.; Szakal, C.; Wucher, A.; Winograd, N. Depth Profiling Studies of Multilayer Films with a C_{60}^+ Ion Source. *Appl. Surf. Sci.* **2004**, *231*–232, 179–182.
- (10) Matsuo, J.; Okubo, C.; Seki, T.; Aoki, T.; Toyoda, N.; Yamada, I. New Secondary Ion Mass Spectrometry (SIMS) System with High-Intensity Cluster Ion Source. *Nucl. Instrum. Methods Phys. Res., Sect. B* **2004**, *219*–220, 463–467.
- (11) Ninomiya, S.; Nakata, Y.; Ichiki, K.; Seki, T.; Aoki, T.; Matsuo, J. Measurements of Secondary Ions Emitted from Organic Compounds Bombarded with Large Gas Cluster Ions. *Nucl. Instrum. Methods Phys. Res., Sect. B* **2007**, *256*, 493–496.
- (12) Yamada, I.; Matsuo, J.; Toyoda, N.; Aoki, T.; Jones, E.; Insepov, Z. Non-Linear Processes in the Gas Cluster Ion Beam Modification of Solid Surfaces. *Mater. Sci. Eng., A* **1998**, *253*, 249–257.
- (13) Toyoda, N.; Hagiwara, N.; Matsuo, J.; Yamada, I. Surface Smoothing Mechanism of Gas Cluster Ion Beams. *Nucl. Instrum. Methods Phys. Res., Sect. B* **2000**, *161*–163, 980–985.
- (14) Mouhib, T.; Poleunis, C.; Mollers, R.; Niehuis, E.; Defrance, P.; Bertrand, P.; Delcorte, A. Organic Depth Profiling of C_{60} and $C_{60}/$ Phthalocyanine Layers Using Argon Clusters. *Surf. Interface Anal.* **2013**, *45*, 163–166.
- (15) Ninomiya, S.; Ichiki, K.; Yamada, H.; Nakata, Y.; Seki, T.; Aoki, T.; Matsuo, J. Precise and Fast Secondary Ion Mass Spectrometry Depth Profiling of Polymer Materials with Large Ar Cluster Ion Beams. *Rapid Commun. Mass Spectrom.* **2009**, *23*, 1601–1606.
- (16) Rading, D.; Moellers, R.; Cramer, H. G.; Niehuis, E. Dual Beam Depth Profiling of Polymer Materials: Comparison of C_{60} and Ar Cluster Ion Beams for Sputtering. *Surf. Interface Anal.* **2013**, *45*, 171–174.
- (17) Rabbani, S.; Barber, A. M.; Fletcher, J. S.; Lockyer, N. P.; Vickerman, J. C. TOF-SIMS with Argon Gas Cluster Ion Beams: A Comparison with C_{60} . *Anal. Chem.* **2011**, *83*, 3793–3800.
- (18) Ninomiya, S.; Ichiki, K.; Yamada, H.; Nakata, Y.; Seki, T.; Aoki, T.; Matsuo, J. Molecular Depth Profiling of Multilayer Structures of Organic Semiconductor Materials by Secondary Ion Mass Spectrometry with Large Argon Cluster Ion Beams. *Rapid Commun. Mass Spectrom.* **2009**, *23*, 3264–3268.
- (19) Wehbe, N.; Tabarrant, T.; Brison, J.; Mouhib, T.; Delcorte, A.; Bertrand, P.; Moellers, R.; Niehuis, E.; Houssiau, L. TOF-SIMS Depth Profiling of Multilayer Amino-Acid Films Using Large Argon Cluster Ar_n^+ , C_{60}^+ and Cs^+ Sputtering Ions: A Comparative Study. *Surf. Interface Anal.* **2013**, *45*, 178–180.
- (20) Mroz, P.; Pawlak, A.; Satti, M.; Lee, H.; Wharton, T.; Gali, H.; Sarna, T.; Hamblin, M. R. Functionalized Fullerenes Mediate Photodynamic Killing of Cancer Cells: Type I Versus Type II Photochemical Mechanism. *Free Radical Biol. Med.* **2007**, *43*, 711–719.
- (21) Ricco, M.; Belli, M.; Mazzani, M.; Pontiroli, D.; Quintavalle, D.; Janossy, A.; Csanyi, G. Superionic Conductivity in the Li_4C_{60} Fulleride Polymer. *Phys. Rev. Lett.* **2009**, *102*, 145901.
- (22) Shaheen, S. E.; Brabec, C. J.; Sariciftci, N. S.; Padinger, F.; Fromherz, T.; Hummelen, J. C. 2.5% Efficient Organic Plastic Solar Cells. *Appl. Phys. Lett.* **2001**, *78*, 841–843.
- (23) Kaskhedikar, N. A.; Maier, J. Lithium Storage in Carbon Nanostructures. *Adv. Mater.* **2009**, *21*, 2664–2680.
- (24) Basiuk, E. V.; Zauco, E. A.; Basiuk, V. A. Chemical Crosslinking in C_{60} Thin Films. In *Micromanufacturing and Nanotechnology*; Mahalik, N. P., Ed.; Springer-Verlag: Berlin, Heidelberg, Germany, 2006; pp 453–462.
- (25) Girifalco, L. A. Molecular Properties of C_{60} in the Gas and Solid Phases. *J. Phys. Chem.* **1992**, *96*, 858–861.
- (26) Hobday, S.; Smith, R.; Gibson, U.; Richter, A. Ion Bombardment of C_{60} Films. *Radiat. Eff. Defects Solids* **1997**, *142*, 301–318.
- (27) Anders, C.; Kirihata, H.; Yamaguchi, Y.; Urbassek, H. M. Ranges and Fragmentation Behavior of Fullerene Molecules: A Molecular-Dynamics Study of the Dependence on Impact Energy and Target Material. *Nucl. Instrum. Methods Phys. Res., Sect. B* **2007**, *255*, 247–252.
- (28) Shinya, T.; Kirihata, H.; Yamaguchi, Y.; Yasumatsu, H.; Kondow, T.; Urbassek, H. M.; Gspann, J. Molecular Simulations of Cluster Ejection by CO_2 Cluster Impact on Carbon-based Surfaces. *Nucl. Instrum. Methods Phys. Res., Sect. B* **2009**, *267*, 3080–3083.
- (29) Webb, R. P.; Garrison, B. J.; Vickerman, J. C. The Effect of the H:C Ratio on the Sputtering of Molecular Solids by Fullerenes. *Surf. Interface Anal.* **2011**, *43*, 116–119.
- (30) Garrison, B. J. Molecular Dynamics Simulations, the Theoretical Partner to Static SIMS Experiments. In *TOF-SIMS: Surface Analysis by Mass Spectrometry*; Vickerman, J. C., Briggs, D., Eds.; Surface Spectra Ltd. and IM Publications: Manchester, U.K., 2001; pp 223–257.
- (31) Wilson, W. D.; Haggmark, L. G.; Biersack, J. P. Calculations of Nuclear Stopping, Ranges, and Straggling in the Low-Energy Region. *Phys. Rev. B* **1977**, *15*, 2458–2468.
- (32) Allen, M. P.; Tildesley, D. J. *Computer Simulation of Liquids*; Clarendon Press: Oxford, U.K., 1991; pp 6–20.
- (33) Stuart, S. J.; Tutein, A. B.; Harrison, J. A. A Reactive Potential for Hydrocarbons with Intermolecular Interactions. *J. Chem. Phys.* **2000**, *112*, 6472–6486.
- (34) Brenner, D. W. Empirical Potential for Hydrocarbons for Use in Simulating the Chemical Vapor Deposition of Diamond Films. *Phys. Rev. B* **1990**, *42*, 9458–9471.
- (35) Czerwinski, B.; Postawa, Z.; Garrison, B. J.; Delcorte, A. Molecular Dynamics Study of Polystyrene Bond-Breaking and Crosslinking Under C_{60} and Ar_n Cluster Bombardment. *Nucl. Instrum.*

Methods Phys. Res., Sect. B 2013, DOI: <http://dx.doi.org/10.1016/j.nimb.2012.11.030>.

- (36) Garrison, B. J.; Postawa, Z. Computational View Of Surface Based Organic Mass Spectrometry. *Mass Spectrom. Rev.* 2008, 27, 289–315.
- (37) Czerwinski, B.; Rzeznik, L.; Paruch, R.; Garrison, B. J.; Postawa, Z. Effect of Impact Angle and Projectile Size on Sputtering Efficiency of Solid Benzene Investigated by Molecular Dynamics Simulations. *Nucl. Instrum. Methods Phys. Res., Sect. B* 2011, 269, 1578–1581.
- (38) David, W. I. F.; Ibberson, R. M.; Dennis, T. J. S.; Hare, J. P.; Prassides, K. Structural Phase Transitions in the Fullerene C₆₀. *Europhys. Lett.* 1992, 18, 219–225.
- (39) Smith, R.; Hobday, S.; Webb, R. Simulation of Energetic Particle-Surface Impacts Involving Fullerenes. *AIP Conf. Proc.* 1997, 392, 515–518.
- (40) Kolomenskii, A. A.; Szabadi, M.; Hess, P. Laser Diagnostics of C₆₀ and C₇₀ Films by Broadband Surface Acoustic Wave Spectroscopy. *Appl. Surf. Sci.* 1995, 86, 591–596.
- (41) Kennedy, P. E.; Garrison, B. J. Chemical Damage Resulting from 15 keV C₆₀, Ar₁₈, and Ar₆₀ Cluster Bombardments of Solid Benzene. *Surf. Interface Anal.* 2013, 45, 42–45.
- (42) Postawa, Z.; Czerwinski, B.; Szewczyk, M.; Smiley, E. J.; Winograd, N.; Garrison, B. J. Enhancement of Sputtering Yields Due to C₆₀ Versus Ga Bombardment of Ag{111} As Explored by Molecular Dynamics Simulations. *Anal. Chem.* 2003, 75, 4402–4407.
- (43) Postawa, Z.; Czerwinski, B.; Szewczyk, M.; Smiley, E. J.; Winograd, N.; Garrison, B. J. Microscopic Insights into the Sputtering of Ag{111} Induced by C₆₀ and Ga Bombardment. *J. Phys. Chem. B* 2004, 108, 7831–7838.
- (44) Rzeznik, L.; Czerwinski, B.; Garrison, B. J.; Winograd, N.; Postawa, Z. Microscopic Insight into the Sputtering of Thin Polystyrene Films on Ag{111} Induced by Large and Slow Ar Clusters. *J. Phys. Chem. C* 2008, 112, 521–531.
- (45) Delcorte, A.; Garrison, B. J.; Hamraoui, K. Dynamics of Molecular Impacts on Soft Materials: From Fullerenes to Organic Nanodrops. *Anal. Chem.* 2009, 81, 6676–6686.
- (46) Postawa, Z.; Paruch, R.; Rzeznik, L.; Garrison, B. J. Dynamics of Large Ar Cluster Bombardment of Organic Solids. *Surf. Interface Anal.* 2013, 45, 35–38.